Proceedings of ASME Turbo Expo 2011
GT2011
June 6-10, 2011, Vancouver, British Columbia, Canada

GT2011-45977

AERODYNAMIC AND AEROTHERMAL INVESTIGATION OF THE FLOW AROUND AN HPT ROTOR SHROUD: PIV MEASUREMENTS

Knut Lehmann, Vasudevan Kanjirakkad, Howard Hodson
Whittle Laboratory, University of Cambridge
Cambridge CB3 0DY, UK

ABSTRACT

An experimental study has been conducted to investigate the aerothermal performance of a shrouded high pressure turbine blade in a large scale rotating rig. The rotor blade and the associated shroud and casing geometry have been modelled in a large scale low speed turbine rig that was designed to investigate a novel passive shroud cooling methodology.

The objective of the present paper is to provide a detailed description of the flow field around the rotor blade shroud. The improved physical understanding of the shroud flow gained from this study will be used to analyse the aerothermal performance of the shroud cooling strategy as reported in a companion paper, Lehmann et al. [1].

Experiments have been carried out using endoscopic PIV to identify and understand salient flow features that exist upstream and downstream of the shroud as well as within the shroud cavities. The measurements are complemented by steady and unsteady numerical computations of the turbine stage. The study identifies the existence of important vortical structures within the shroud cavities that not only interact with the main passage flow but also modify the amount and distribution of the shroud leakage flow in a manner that has major implications for shroud cooling and heat transfer. A detailed shroud flow model is derived and used to elucidate the causes and consequences of the flow pattern observed. The model emphasises the circumferentially asymmetric nature of the cavity flow structures caused by the presence of the inter shroud gap that in turn influences the production, interaction and dissipation of such vortical structures.

NOMENCLATURE

Greek symbols

μ	Dynamic viscosity	[Pa s]
ρ	Density of air	[kg m^{-3}]
φ	Flow coefficient	[-]

Latin symbols

C_{stator}	Stator midspan chord	[mm]
C_{rotor}	Rotor midspan chord	[mm]
C_p	Pressure coefficient $\left(p_{01\infty}-p\right)/0.5\rho(v_{x1\infty}/\cos(70))^2$	
$\dot{m}$	Mass flow rate	[kg s^{-1}]
Re	Reynolds number	[-]
U	Blade speed at midspan	[ms^{-1}]
V	Velocity, absolute	[ms^{-1}]
W	Velocity, relative	[ms^{-1}]

Subscripts

$_0$	stagnation value
$_1$	at stator inlet
$_2$	at rotor inlet
$_3$	at rotor exit
$_r$	radial
$_x$	axial
$_\theta$	circumferential

INTRODUCTION

The shrouded HPT rotor blade with a multiple seal arrangement in the over-tip leakage path can have significant aerodynamic advantages over its shroudless counterpart as the tip leakage flow can be generally reduced, especially in low reaction stages. Most shroud related research is concerned with turbine performance and the effects of shroud inlet/exit cavity flows, e.g. Pfau et al.[2], Porreca et al. [3], Rosic et al. [4].

Pfau et al. [2] report potential benefits from the net leakage into the shroud inlet cavity through the removal of low momentum fluid and a consequent reduction in rotor secondary flow. Gier et al. [5] show that the mere presence of the shroud cavities causes significant interaction between the main flow and the cavity flow. The parametric study shroud cavity geometries of Rosic [4] stresses the importance of small volumes for the inlet and exit cavities in order to reduce mixing losses. Giboni et al. [6] carried out detailed measurements and computations of the shroud exit cavity flow revealing cavity vortex and secondary flow interactions and the part played by shroud leakage jet on imparting negative incidence on to the downstream stator.

Kanjirakkad et al. [7] and Janke et al. [8] have investigated passive shroud cooling concepts, by assessing adiabatic cooling effectiveness, in an attempt to avoid thick shrouds with active internal and film cooling.

Waschka et al. [9] and Wittig et al. [10] have experimentally studied stepped labyrinth seals and report on cavity flow structures and heat transfer. More recently Haller and Hilditch [11] and Lehmann et al. [12] reported heat transfer distributions over the shroud surfaces. This and the adiabatic cooling effectiveness are the two most important parameters required by the thermal engineer for a successful cooling design.

It is evident from the above studies that the aerodynamic performance and cooling requirements of the shroud greatly depend on the detailed flow structures that exist around it and within the cavities. Although the existing literature discusses the shroud flow aerodynamics to varying degrees of detail, it is apparent that the local flow structures are largely influenced by and are a result of the specific shroud geometry under consideration.

In the present paper detailed flow structures of the shroud geometry presented in Kanjirakkad et al. [7] and Lehmann et al. [12] is studied in depth by means of experiments using endoscopic PIV. One important aspect of this study is the modelling of the inter-shroud gap in the rotor blade tip region. It will be shown that this gap has a major influence on the local aerodynamics around the shroud. The experiments are supplemented with steady and time averaged unsteady CFD results. A detailed shroud flow model is derived from the observations made in this study. This flow model is widely used in the companion paper, Lehmann et al. [1], to explain the heat transfer and cooling effectiveness distributions around the shroud.

EXPERIMENTAL METHOD

Configuration of the research turbine

The large-scale low-speed research turbine at the Whittle Laboratory, also known as the Peregrine rig, was used to perform an experimental study of the rotor shroud flows in a single stage shrouded HPT configuration. The principal layout of the test section is sketched in Figure 1. Some important geometrical parameters as well as the operating conditions of the turbine are listed in Table 1.

A large variable speed suction fan pulls the flow though the turbine stage. The power generated by the turbine is absorbed by an eddy current brake, which in turn is used to control the rotational speed of the turbine rotor. The fan and brake are in a control loop such that the rig operating condition (Re and φ) is accurately controlled within ±0.5% during an experiment.

The stage consists of 26 stator and 45 rotor blades. Each rotor blade carries a shroud with three forward leaning fins. Inter-shroud gaps of 1.3mm width separate the individual rotor

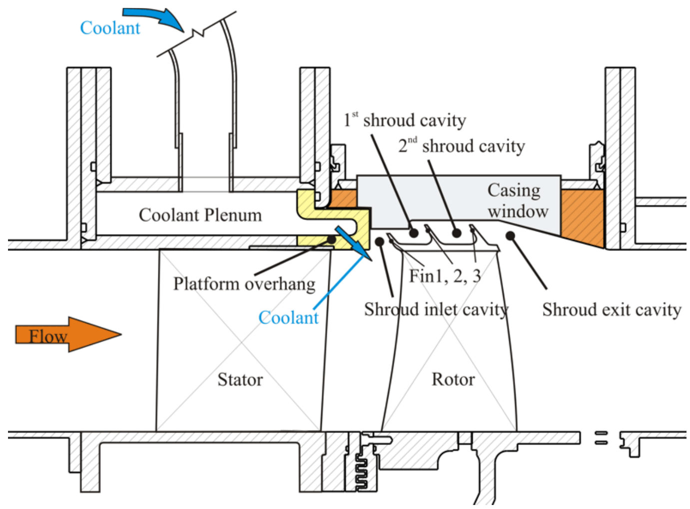

Figure 1 Schematic of the research turbine

Number of stages	1
Number of stator blades	26
Number of rotor blades	45
Mean radius [m]	0.6858
Hub-tip radius ratio	0.8
Stator chord (mid-span) [mm]	225
Rotor chord (mid-span) [mm]	120
Rotor tip clearance (nominal) [%span]	1.4
Inter-shroud gap size (nominal) [mm]	1.3
Number of coolant holes	260
Coolant hole diameter [mm]	4
Coolant flow rate $m_{\%cool}=m_{cool}/m_{inlet}$ x100	0%
Flow coefficient $\varphi=V_{x1}/U$	0.42
Re (nominal) Re=$\rho_1(V_{x1}/\cos 70°)C_{stator}/\mu$	5x10^5
Re (rotor based) Re$_R$=$\rho_3 W_3 C_{rotor}/\mu$	2.5x10^5
Rotational speed [rpm]	~360
Near-casing Stator flow angles (inlet/exit) [°]	0° / 67°
Near-casing Rotor flow angles (inlet/exit) [°]	-2° / -62°

Table 1 Geometrical parameters and test conditions

shrouds in the circumferential direction. The rotor casing above the shroud consists of a parallel annulus with a backward facing step in front of the first and the second fin.

The stage configuration features the passive 'through platform' cooling concept (Kanjirakkad [7]). Coolant air is ejected through 260 circular holes in the stator platform overhang downstream at a tangential angle of 65° with a radial compound angle of 30°. The cooling concept is intended to cool the over-shroud region as well as the shroud underside. However, the measurements reported in this paper were obtained for an uncooled condition. The effects of the coolant flow are discussed in the companion paper Lehmann et al. [1].

PIV measurement technique

One of the main foci of this research is a study of the flow field around the turbine shroud. The flow features in the shroud cavities are of primary interest as they are strongly related to the heat transfer pattern on the shroud. However, the acquisition of flow field information in the narrow shroud cavities is a difficult task, primarily due to the limited access available and the associated difficulties of traversing aerodynamic probes. Furthermore, the confines of such narrow space raise the question of measurement tool intrusion and the associated impact on the flow. The need to traverse a probe and the direct intrusion of the probe tool at the measurement plane can be avoided using the Particle Image Velocimetry (PIV) measurement technique.

The implementation of PIV to measure the flow in the rotor shroud cavities requires the use of miniature endoscopy. A PIV system from LaVision was used which provides this capability. The laser hardware comprises a double rod Nd-YAG laser of type New Wave SOLO 120, an articulated laser delivery arm and the laser optics. The PIV camera used has a 12 bit CCD chip with a resolution of 1280 x 1024 pixels. It can be equipped with a 10mm diameter endoscope and an additional mirror sleeve to rotate the field of view by 90°.

A schematic of the experimental setup in the turbine rig is shown in Figure 2a. A narrow section of the rotor casing was modified and equipped with a small glass window. This allows a cross section of the shroud cavities to be illuminated with the laser sheet. The 90° camera endoscope is used to provide a view that is normal to the laser sheet. Several holes were accommodated into the rotor casing at different axial positions to access all four shroud cavities as well as the region downstream of the rotor blades. In all cases, the camera endoscope is situated about 7 endoscope diameters tangentially downstream of the measurement plane. Thus, a potential interference with the cavity flow field is avoided.

The seeding particles were produced with a Le Maitre G100 smoke generator. In order to seed the over shroud leakage flow, it proved to be most effective to eject the smoke through the cooling holes in the stator casing. Unfortunately, this prevented measurements at precisely zero percent coolant flow

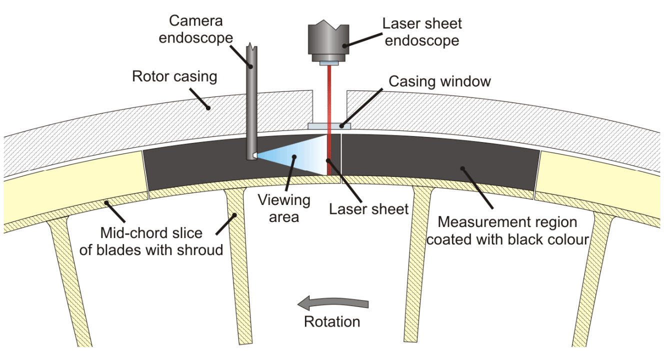

a) Schematic of the PIV setup in the turbine rig

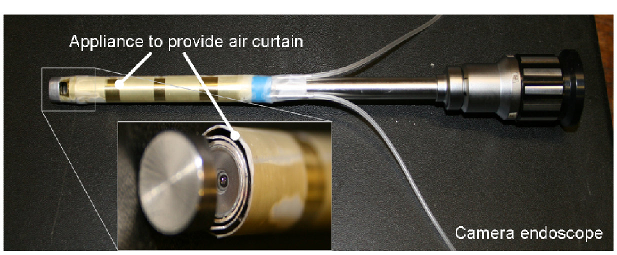

b) Modified camera endoscope to avoid seeding condensation

Figure 2 PIV setup in the turbine rig

rate. However, the seeded coolant flow was restricted with an orifice plate to a very low mass flow rate. Thus, it is assumed that these experiments are a good approximation of the uncooled case.

One major disadvantage of using the camera endoscope in the described manner is the condensation of the smoke on the endoscope mirror. Even small amounts of condensation render the acquired PIV images useless. This problem has proven to be most serious in the shroud cavities where the endoscope is directly facing the swirling cavity flow. To mitigate this problem, a thin piece of sheet metal was mounted around the tip of the endoscope leaving a small cavity between both parts (Figure 2b). By blowing pressurised air through this cavity, an air curtain was formed that effectively shielded the endoscope mirror from the smoke particles. Several PIV experiments were performed to assure that the air curtain had no effect on the flow field under investigation.

Due to the complicated experimental setup, the PIV measurements were only performed at one fixed position relative to the stator blade row (The position is shown in Figure 4). However, any rotor relative position could be easily achieved by triggering the acquisition of the PIV system accordingly. In the present study, one rotor pitch was covered with 16 equidistantly spaced measurement planes. This corresponds to a spacing of 0.5°. Additional measurements were taken to achieve a resolution of 0.25° in the vicinity of the inter-shroud gaps. Around 120 images for each rotor relative position, have proven adequate in order to obtain phase averaged results. Several tests with 240 averaged images showed no discernable differences in the results.

The acquired particle images were post processed using the LaVision software DaVis 7.1. An adaptive multi pass algorithm was used with an initial interrogation window of 64 x 64 pixels decreasing to a final interrogation window of 16 x 16 pixels with 50 % window overlap. Thus, a vector grid spacing of 380 µm was achieved. No smoothing was applied to the final vector field.

NUMERICAL METHOD

The computational mesh for the present study was created using the CENTAUR mesh generator. A schematic of the computational domains is shown in Figure 3a. The computational mesh consists of the stator and the rotor domain. The coolant holes, including the coolant plenum, are part of the stator domain. The mesh is unstructured with highly resolved prismatic layers near the viscous walls. The y^+ value on the blades is less than 1.3 throughout. The total mesh size is approximately 10.5 million cells equally shared between the stator and the rotor domain. Detailed views of the computational mesh in the tip sections of the stator and rotor domains are presented in Figure 3b and c. The rotor domain has a refined mesh with an increased cell density near the rotor shroud.

The commercial software package FLUENT 6.3 was used in order to obtain solutions of the flow field. The solver was run in the compressible mode with a pressure based formulation for the equations. The relizable k-ε turbulence model was used. In

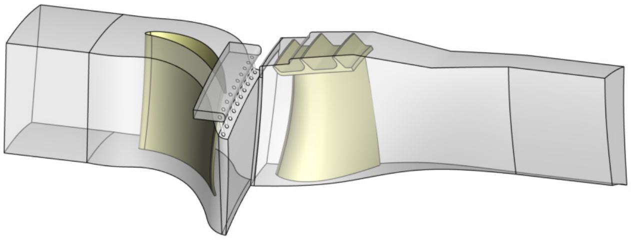

a) Schematic of the computational domain

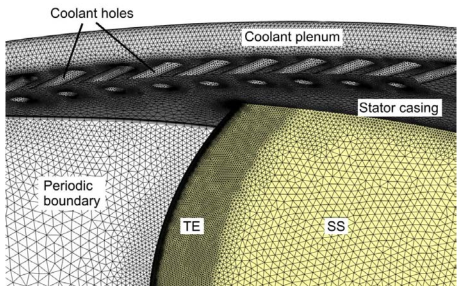

b) Mesh details in the tip section of the stator domain

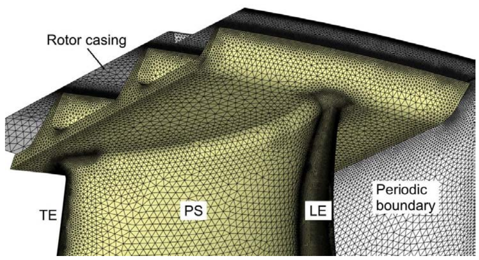

c) Mesh details in the tip section of the rotor domain

Figure 3 Details of the computational mesh

the case of the steady state calculations, a mixing plane was employed to couple the stationary with the rotating domain.

A particular interest of the computational study was the interaction of the flow at the shroud inlet cavity. The steady state calculations have the disadvantage of the mixing plane, preventing the potentially important stator pressure field to affect the flow at the shroud inlet cavity and in the tip section of the rotor domain. An unsteady calculation is a more realistic approach and can potentially yield more accurate predictions of the flow. In order to perform a time accurate calculation, a sliding plane approach was used to couple the rotor and the stator domain. This required the stator to be scaled up by 15.6 % to give a pitch equal to two rotor pitches. The pitch to chord ratio of the stator blade was kept constant in the scaling process. A new mesh was created in which one stator and two rotors were modeled. This resulted in a total mesh size of approximately 14.9 million cells for the unsteady calculation.

RESULTS AND DISCUSSION

Shroud inlet cavity

An understanding of the local inflow pattern of the shroud inlet cavity is important from an aerothermal point of view as it highlights the regions where hot main passage fluid (or possibly cooled fluid in the cases with coolant flows present) enters the cavity. The outflow behaviour is equally important, especially in the cases with coolant flows present as it determines where potentially highly cooled shroud cavity fluid re-enters the rotor passage.

From an aerodynamic perspective, the shroud inlet cavity flow might have beneficial effects on the secondary flow within the rotor passage (e.g. Pfau et al [2]). This is due to the removal of the highly skewed stator casing boundary layer into the shroud inlet cavity. However, a positive radial migration of stator passage fluid is associated with this net inflow to the cavity. For a typical radial temperature profile at nozzle exit this leads to higher temperatures on the shroud underside.

The inflow/outflow pattern of the shroud inlet cavity is mainly influenced by the pressure fields of the stator and rotor blade and to a lesser extent by the presence of the inter-shroud gap. The circumferential variation of inflow/outflow of the cavity depends on the frame of reference from which the flow is observed. In the absolute frame of reference, only the variations due to the stator pressure field are visible in the time-mean flow as the influence of the rotor is circumferentially averaged.

Figure 4a shows contours of the non dimensional radial velocity at the main passage - shroud inlet cavity interface. The data was extracted from an unsteady CFD calculation and is time averaged in the stationary frame of reference. The cavity flow is characterised by a circumferential band of inflow in the centre region of the cavity interface. Either side of it, negative radial velocities are present. The negative radial velocities near the upstream wall of the inlet cavity are not considered true outflow as the fluid involved is mixing with the shear layer which in turn is instantly drawn back into the cavity. Hence, the outflow occurs only in a narrow axial band near the shroud. A circumferential modulation of the radial velocity at the cavity interface is evident. However, the effect is quite weak. The low pressure region that extends from the suction surface of the stator leads to reduced inflow into the cavity (zone labelled ‘B’). Conversely, the high pressure region near the trailing edge promotes the ingestion of fluid into the cavity (zone labelled ‘A’).

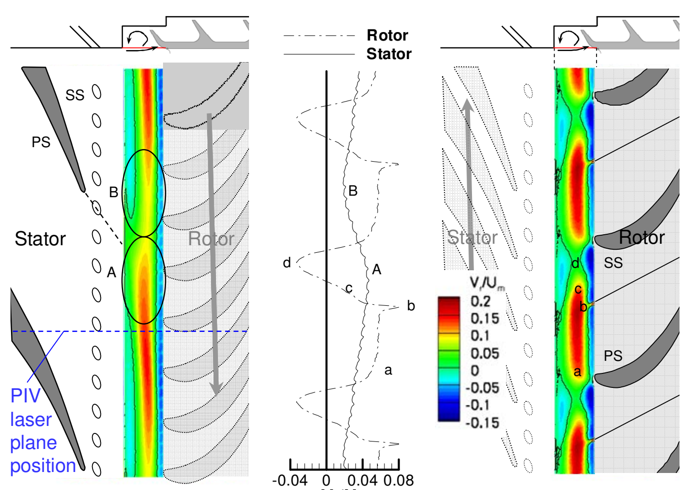

a) b) c)

Figure 4 Time averaged contours of radial velocity at the shroud inlet cavity interface (unsteady CFD) a) Absolute ref. frame; b) Axially averaged line plot; c) Relative ref. frame

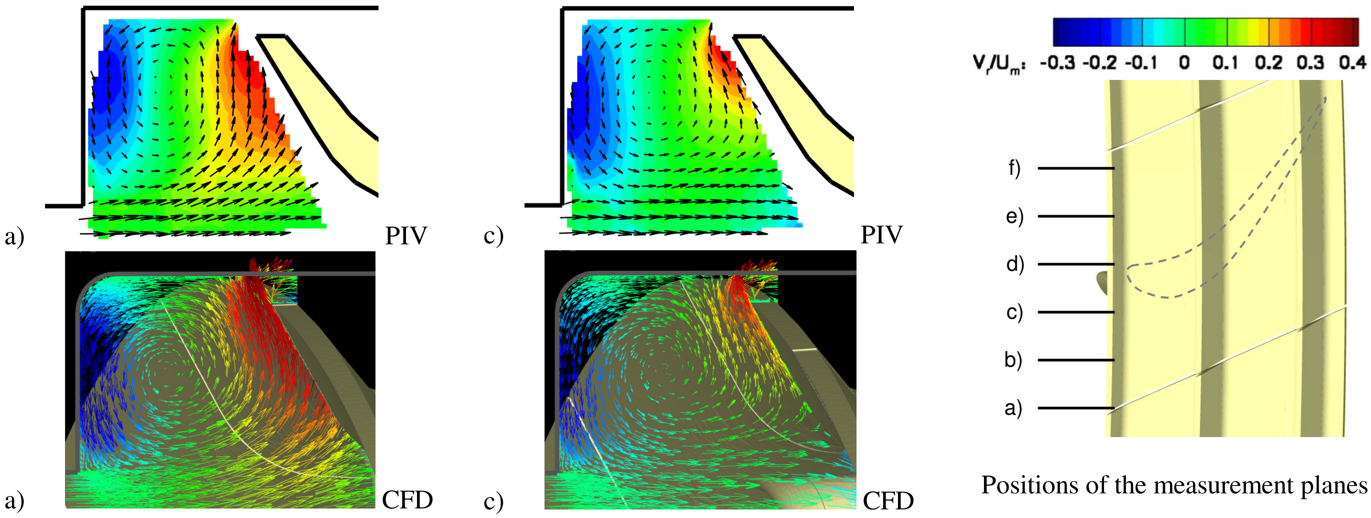

Figure 5 Phase averaged flow vectors at θ=const planes in the shroud inlet cavity (PIV and steady CFD)

Figure 4b shows the radial velocity, axially averaged across the cavity interface in both rotor and stator relative reference frame. In the stator relative frame, there is net inflow at all pitchwise positions with the minimum inflow velocity being less than 40 % of the maximum. The variation in the rotor frame of reference is much stronger. This is due to the strong potential field of its leading edge and the fact that the rotor blade is axially closer to the cavity. Hence, with respect to the aerothermal performance of the rotor shroud, the flow seen from the rotor relative frame is more important. The plots in Figure 4b and c present the results in the rotor relative frame. It can be seen that distinct pitchwise regions of net inflow and outflow exist. In the region near the pressure side, the free shear layer is pushed into the cavity under the action of the high pressure of the rotor blade potential field. The inflow region extends for about 70 % of the rotor pitch from the blade leading edge 'a' towards the suction side of the adjacent blade at position 'c'. The inflow to the cavity peaks in the vicinity of the inter-shroud gap 'b', as the gap presents an additional sink in the downstream wall of the shroud inlet cavity.

It is noted that the inflow region extends quite far towards the suction side of the blade, where a weak inflow (or even outflow) could be expected. This is explained by the strong skew in the free shear layer. The rotor blade pressure field near the tip is mainly established by high momentum main passage fluid that approaches the rotor leading edge axially in the relative frame. The highly skewed flow within the shear layer has low absolute tangential momentum and therefore, in the rotor relative frame, travels against the direction of blade rotation. As this flow passes through the high pressure region near the blade leading edge, it accelerates radially outwards. However, the highest radial velocities are reached only after the fluid has travelled through the high pressure region and therefore the inflow region is stretched in the tangential direction.

The net outflow from the cavity occurs predominantly in the low pressure region near the suction side of the blade at position 'd'. It presents a leakage flow back into the rotor passage. As described previously, the shroud inlet cavity vortex consists mainly of low momentum fluid from the stator casing boundary layer. Therefore, this leakage flow imposes negative incidence on the rotor and is likely to feed into the passage vortex of the rotor. The aerothermal implications of this behaviour, especially on the cooling effectiveness on the shroud underside, are discussed in the companion paper, Lehmann et al. [1].

The PIV results for the phase averaged flow in the shroud inlet cavity are plotted in Figure 5. The flow vectors and contours of radial velocity are given in θ=const planes at 2 rotor relative pitchwise positions corresponding to the maximum and minimum of leakage flow entering the shroud inlet cavity. The CFD results from a steady computation are shown for comparison and agree well with the PIV.

Figure 5 plane a) shows the results near the inter-shroud gap. The vector map shows the large shroud inlet cavity vortex. In agreement with the numerical results in Figure 4c, strong positive radial velocities are observed near the fin. Near the mid-height of the fin, the flow vectors are normal to the fin surface, marking the position where some cavity flow escapes through the inter-shroud gap. Close to the suction side of the leading edge at Figure 5 plane c), the intensity of the cavity vortex is much lower. Induced by the low static pressure in the vicinity of the suction side of the blade, there is a net outflow from the cavity (compare to Figure 4c). This outflow occurs predominantly near the base of Fin 1.

1st Shroud Cavity

The detailed flow structure in the first shroud cavity is discussed with the help of the experimental PIV results. The PIV measurements were taken in meridional (θ=const) planes at various rotor relative pitch-wise positions in the first shroud cavity. Figure 6 planes a)-g) show the vector maps with contours of the radial velocity for the corresponding pitch wise positions. The spacing of the measurement planes is 1.5° near mid-pitch and 0.75° in the vicinity of the inter shroud gaps. For the sake of brevity only some of the CFD results are presented here for comparison. Generally the predicted results were found to be in good agreement with the PIV.

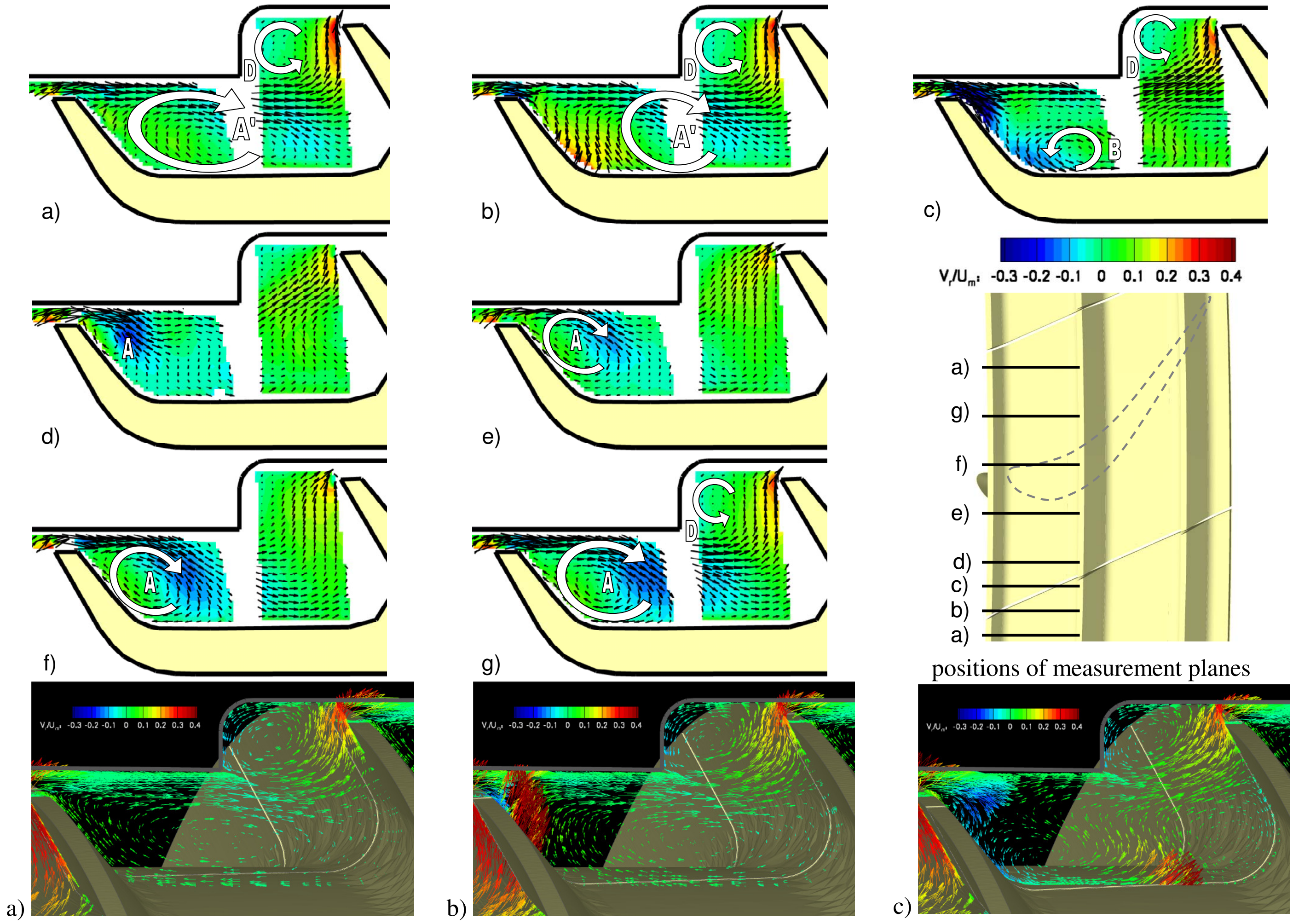

Figure 6 Phase averaged PIV flow vectors at θ=const planes in the first shroud cavity (sub captions refer to measurement plane positions; bottom row figures show steady CFD results for comparison)

Figure 6 plane a) shows a plane on the pressure side of the shroud near the inter-shroud gap. A strong fin tip leakage jet enters the cavity and stays attached to the rotor casing up to the backward facing step. It drives a large recirculation, the cavity vortex A', which occupies almost the entire shroud cavity. At the backward facing casing step, the leakage jet separates. It bends slightly radially inwards and attaches on the front face of Fin 2 further downstream. The majority of this flow is then pulled radially outwards towards the tip gap of Fin 2. A weak recirculation D is formed directly behind the backward facing step.

Figure 6 plane b) shows a cut-plane that includes a part of the inter-shroud gap near Fin 1. High radial velocities are found where leakage flow from the main passage enters the shroud cavity through the inter shroud gap. Apart from that, the cavity flow is very similar to that at plane a). Towards plane c), the inflow through the inter-shroud gap shifts axially downstream. Here the driving pressure for the leakage flow is lower. This results in a weaker inflow at this position.

The flow vectors near the bottom of the cavity show that the inter-shroud gap leakage flow enters the cavity with a positive axial velocity component (plane b) and c)). This is against the direction of the recirculating flow in the shroud cavity vortex A'. In the mixing process of both flows, the shroud cavity vortex A' dissipates.

The leakage flow through the inter-shroud gap also enters the shroud cavity at an absolute tangential velocity that is higher than that of the cavity flow. Thus, the leakage jet from the inter-shroud gap is bent against the direction of blade rotation and partly rolls up into the shroud gap vortex B (see Figure 6 plane c). This vortex is visible at the cavity bottom near the root of Fin 1. The vortex is strong and occupies a region near the shroud gap and very near the surface. It is shown in the companion paper [1] that this vortex is a cause of high heat transfer in this region. The shroud gap vortex B is bound to the inter-shroud gap, and it is no longer visible at plane d). At this plane, the fin tip leakage jet is seen to separate from the casing shortly behind the tip gap and rolls up into a vortex A. The vortex drives the fin tip leakage flow onto the rear face of Fin 1. The impingement of this flow is also associated with very high heat transfer.

As a consequence of the separation from the rotor casing, the fin tip leakage jet diffuses in the cavity and is not carried over to attach at the front face of Fin 2. This results in a smoother sink flow into the tip gap of Fin 2 at planes d), e) and f). The details and consequences on the leakage mass flow rate over Fin 2 are discussed below.

The vortex A that is created by the fin tip leakage jet grows towards plane e) and further towards planes f), g) and a) where it becomes the large shroud cavity vortex. In each successive plane, the separation of the fin tip leakage jet from the casing and also the attachment on the shroud occur closer to the second fin. Only near the shroud pressure side does the fin tip leakage jet impinge directly on the front face of Fin 2. At this position, the shroud cavity vortex fills the entire shroud cavity. The flow in the cavity is fully developed and looks similar to the circumferentially uniform flow that is found in the absence of inter shroud gaps. The flow structure in the first shroud cavity is summarised in Figure 13.

Effect of cavity flow structure on the fin tip leakage flow

As indicated in the previous section, the local shroud cavity flow structure has an influence on the local discharge coefficient in the tip gap of Fin 2. In the absence of the inter shroud gaps, the cavity flow is almost circumferentially uniform. In this case, the separated region on the fin tip and the local discharge coefficient do not vary much in the pitch wise direction. Some evidence for this is presented in Figure 7 which shows the radially averaged axial velocity in the tip gap of Fin 2 over one blade pitch. The circumferential positions of the PIV planes are labelled as in Figure 6.

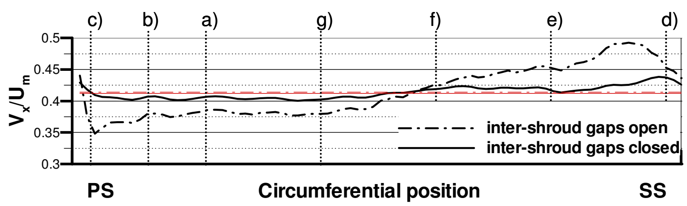

Figure 7 Radially averaged axial velocity in the tip gap of Fin 2 (steady CFD) (red lines are averages)

In the absence of the inter-shroud gaps, the circumferential variation in the tip leakage flow is very small. With their presence however, the local tip leakage mass flow varies significantly. At the pressure side of the shroud (planes c, b, a and g) the leakage flow is lower and on the suction side (planes f, e, and d) the leakage flow is higher compared to the case with no inter shroud gaps. The circumferential average, i.e. the total fin tip leakage mass flow is almost identical in both cases.

The decisive factor that affects the discharge behaviour is the location of the attachment point of the tip leakage jet from Fin 1. As in the case without shroud gaps, the attachment point is close or even at the front face of Fin 2 near the pressure side of the shroud. Thus, the flow follows the front face of Fin 2 as it approaches the tip gap. It reaches the tip gap with a high radial and even negative axial velocity as shown in Figure 6 plane a). This results in a relatively large separation at the fin tip and, hence, a smaller discharge coefficient and, consequently, a lower tip leakage flow.

Due to the small size of the cavity vortex at the positions d, e and f, the fin tip leakage jet attaches near the rear face of Fin 1. Its axial momentum dissipates in the cavity. The result is a much smoother and more uniform sink flow towards the tip of Fin 2 that attracts fluid from a larger region as shown in Figure

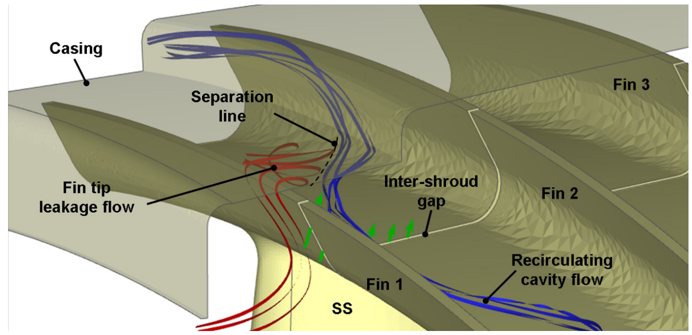

Figure 8 Rollup mechanism of the shroud cavity vortex (streamlines from steady CFD)

6 plane e). The intended benefit of the inclined fin cannot be exploited in this situation and the discharge coefficient is about 20 % higher compared to the pressure side.

Mechanism for the separation of the fin tip leakage jet and rollup into the cavity vortex

It was shown in Figure 6 that the fin tip leakage jet starts to roll up into a vortex near the suction side corner tip of Fin 1. The separation from the casing and the rollup is triggered by the leakage flow from the inter-shroud gap. The mechanism is illustrated in Figure 8.

The leakage flow from the inter-shroud gap (green arrows) presents a blockage to the recirculating cavity flow. The cavity flow (blue streamlines) accelerates tangentially as it is displaced radially from the shroud towards the casing. Near the casing, this flow has a high tangential velocity. This flow meets the tip leakage jet from Fin 1 (red streamlines) that enters the shroud cavity almost axially. Where the opposing flows meet, the leakage jet from Fin 1 separates from the casing and rolls up into the shroud cavity vortex. The separation line on the casing shifts axially downstream and towards the pressure side of the shroud as more tip leakage flow is entrained in this vortex. The trajectory of the separation line is dependent on the relative tangential velocity in the shroud cavity. Higher relative tangential velocities lead to smaller angles between the fin and the separation line and vice versa.

2nd shroud cavity

Similar to the flow in the first shroud cavity, the flow in the second shroud cavity is mainly influenced by a fin tip leakage jet and leakage flow form the inter-shroud gap. Therefore it might be expected that similar blade periodic flow structures

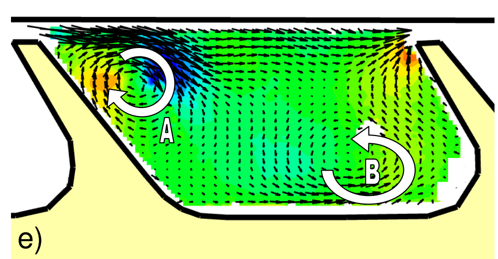

Figure 9 Phase averaged flow vectors a θ = const plane in the second shroud cavity (PIV)

develop in this cavity. This was confirmed by the results of the PIV experiments. For brevity, the results of the PIV measurements are shown only in one plane of the second shroud cavity (see Figure 9). The relative pitchwise position of the measurement plane is identical to that of plane e) in Figure 6.

The flow vectors in Figure 9 show the fin tip leakage jet separating from the casing and rolling up into the shroud cavity vortex A. The mechanism is identical to that in the first shroud cavity, shown in Figure 8. A main difference to the first shroud cavity is the larger volume of the second shroud cavity due to greater radial extent of the fins. This gives vortex A more space to dissipate within the shroud cavity and hence its impact on the near wall flow is lower. It is shown in the companion paper ([1]) that this implies lower Nusselt numbers on the shroud surfaces in the second cavity.

Shroud exit caviy

As mentioned in a previous section, the shroud exit cavity flow is expected to be influenced by rotor pressure field and vice versa. Various authors (e.g. Pfau et al. [2], Rosic et al. [4] and Rushton [13]) have reported a rotor periodic modulation of the shroud exit cavity flow with inflow and outflow from the shroud exit cavity. The rotor blade pressure field acts on the shroud exit cavity flow. Similarly, the exit cavity flow structures modify the local pressure field at the cavity interface. In order to elucidate the cause and effect of the resulting flow an “undisturbed” rotor blade pressure field is first considered. Figure 10a shows a plot of the static pressure coefficient (steady CFD) at 90 % span, a radial location that is only slightly influenced by the cavity flow. As expected, the plot shows a low pressure region that extends downstream near the suction side of the blade. This low pressure region attracts fluid from the shroud exit cavity. Conversely, main passage fluid is pushed into the cavity under the action of the high pressure region that is present in the vicinity of the blade trailing edge.

Figure 10b and c show the pressure field and the normalised radial velocity directly at the main passage - exit cavity interface (100 % span). The radial velocity contours in Figure 10c reveal a strong circumferentially alternating inflow and outflow at the shroud cavity just downstream of the shroud trailing edge. The inflow/outflow regions correlate with the rotor pressure field at 90 % span suggesting that the blade potential field is the main cause of this radial flow. The radial momentum builds up as the fluid travels through the high/low pressure regions, resulting in inflow/outflow zones that are stretched in the streamwise direction.

Figure 10b shows that the pressure field at the cavity interface is significantly different from that at 90 % span. Regions of radial velocity, that are greater and smaller than 5 % of blade speed, are marked by two contour lines. A distinct low pressure zone is located between the inflow and outflow regions. It marks the core of a vortex that develops just downstream of the trailing edge. This shroud trailing edge vortex plays a major role in the mixing process between the main passage and the shroud exit cavity flows. Its development and further implications are discussed below with the help of PIV results and CFD.

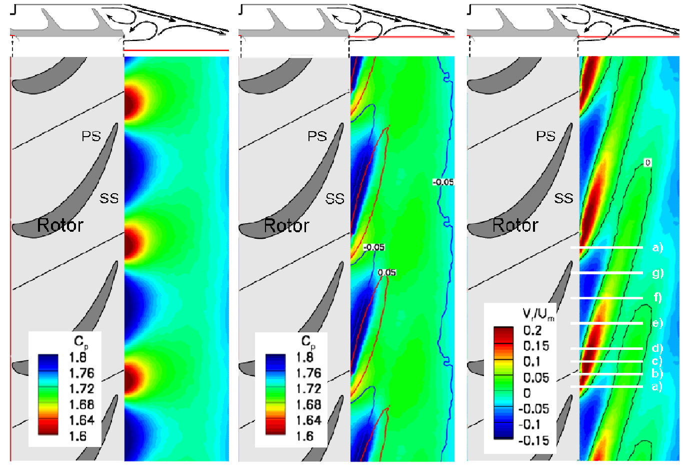

a) b) c)

Figure 10 Flow interaction at the shroud exit cavity (CFD); a) Cp at 90 % span; b) Cp at cavity interface (100 % span); c) Radial velocity at cavity interface (PIV planes marked)

The results from the PIV experiments in the shroud exit cavity are shown in Figure 11 planes a)-g). The phase averaged flow field is presented in θ=const planes at 7 different rotor relative positions in the shroud exit cavity. The predicted results show good agreement and are plotted in extracts in Figure 11.

Plane a) is located near the pressure side edge of the shroud. At this position, fluid from the cavity is ejected into the main passage. Relative to the rotor blade this ejection occurs at the suction side of the rotor wake. Due to the secondary flows in the rotor passage, the suction side part of the rotor wake is already associated with negative radial velocities. Some of the cavity flow feeds into this region. Furthermore, traces of two large vortices A’ and C’ are present in the cavity. A’ and C’ are the remainders of the shroud cavity vortex and the shroud trailing edge vortex respectively. Both vortices have started to develop near the suction side edge of the shroud.

Plane b) shows a position containing the inter shroud gap near the root of Fin 3. The gap leakage flow is ingested into the cavity with positive radial and axial momentum. This results in an axial displacement of vortex A’ away from Fin 3. Near the shroud trailing edge, the main passage flow starts to enter the shroud cavity. The inflow is driven by the high pressure zone of the rotor trailing edge (Figure 10a). Furthermore, in the aft tip region of the blade passage, the rotor secondary flow causes a positive radial migration of fluid on the pressure side of the blade. This migration continues after the wake is shed from the blade and thus enhances the radial inflow to the shroud cavity at this position. Towards plane c), the inflow becomes stronger. The tight streamline curvature results in a low pressure region just downstream of the shroud trailing edge (see Figure 10b). This low pressure region in turn promotes a spiralling motion of the ingested flow and the subsequent rollup into the shroud trailing edge vortex C.

Near Fin 3, the flow behaves in a very similar way to the flow behind Fin 1 and Fin 2 in the first and second shroud cavities respectively. One consequence of the inter-shroud gap leakage flow is the separation of the tip leakage jet and its subsequent rollup that starts the fresh shroud cavity vortex A. At

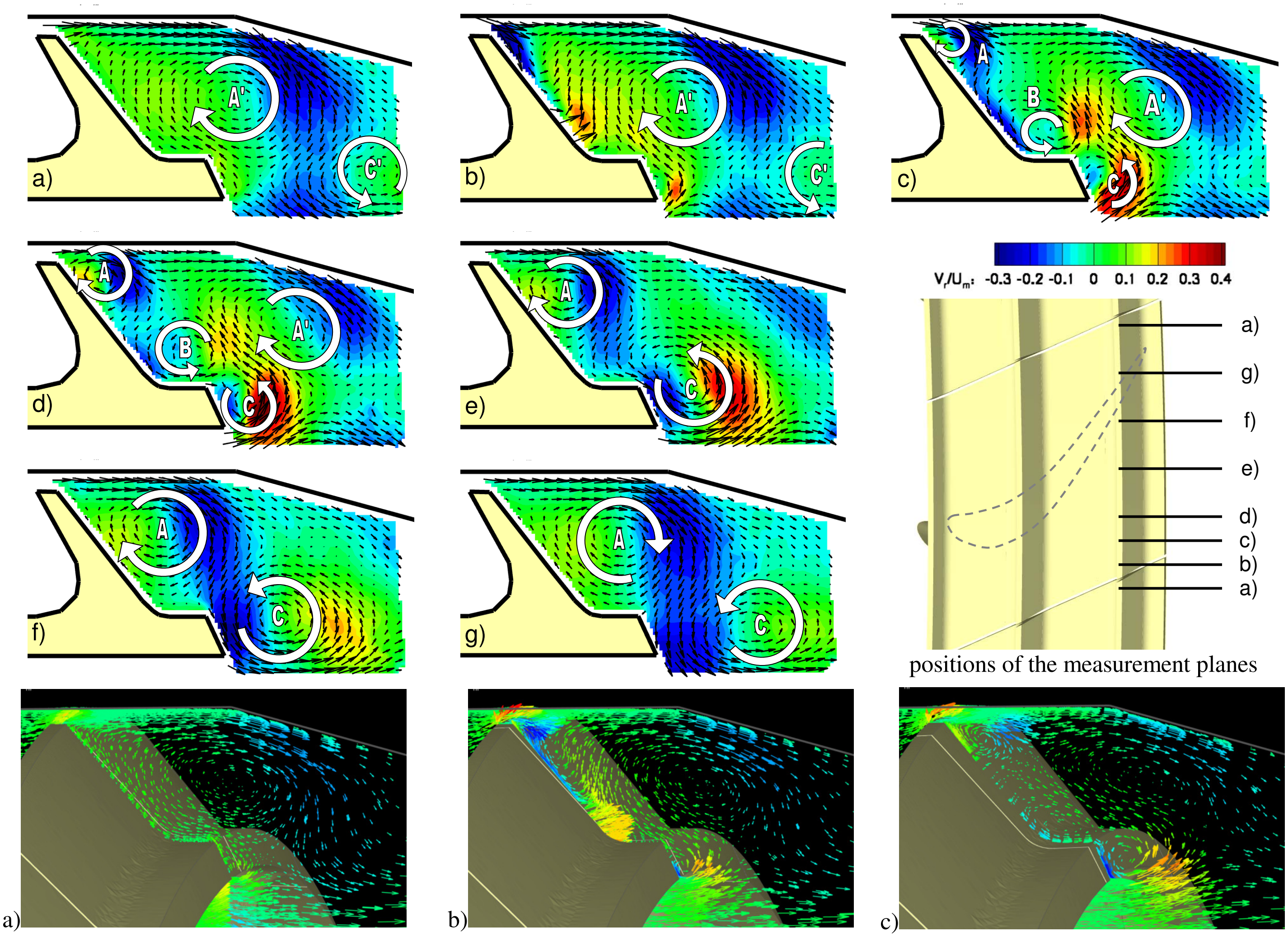

Figure 11 Phase averaged PIV flow vectors at θ=const planes in the shroud exit cavity (captions refer to measurement plane positions; bottom row figures shows steady CFD results for comparison)

plane c) the vortex is small but very intense. It tightly bends the fast fin tip leakage jet such that it impinges near the tip on the rear surface of Fin 3. High rates of heat transfer are driven by this flow (see companion paper Lehmann et al. [1]). Furthermore, a small shroud gap vortex B, similar to that in the first and second shroud cavity, is formed.

The shroud trailing edge vortex C is further developed and bigger at plane d). Just downstream the shroud trailing edge, it drives cavity fluid back into the main passage. On its downstream side, this vortex interacts with the cavity vortex A' that had developed from the previous shroud. Both vortices support the migration of main passage flow deeper into the shroud cavity. Further towards the mid pitch position of the shroud at planes e) and f), the old shroud cavity vortex A' becomes weak and dissipates. Only the new shroud cavity vortex A and the shroud trailing edge vortex C remain. The growing shroud cavity vortex A induces negative radial velocities on its downstream side. Its growth and the attachment position of this flow on the fin surface are well reflected in the flow visualisation and the heat transfer results. At planes f) and g), the effects of the two counter rotating vortices combine and amplify the induction of negative radial velocities between them. In this process, large amounts of cavity fluid re enter the main passage just downstream the shroud trailing edge.

The detrimental effects of the vortex system in the shroud exit cavity concern both the thermal and the aerodynamic performance. From the thermal point of view, the shroud cavity vortex A and the high heat transfer that is caused by its attachment on Fin 3 is of highest importance (see companion paper [1]). However, further CFD calculations with closed inter-shroud gaps suggest that its significance in the mixing of the exit cavity flow and the main passage flow is low. The main driver that influences the mixing process of the main passage flow and the leakage flow is the shroud trailing edge vortex C. Since its development is caused by the potential field of the rotor blade, it is largely insensitive to flow from the inter-shroud gap.

As observed in Figure 10c, the highest radial velocities at the interface of the main passage and the shroud cavity are found just downstream of the shroud trailing edge. However, the flow along the shroud underside has no radial momentum as it leaves the shroud underside parallel to the wall. Hence, the

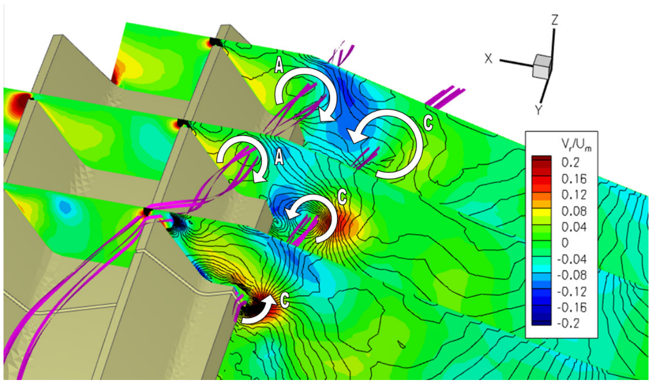

a) Radial velocity in θ = const planes in the shroud exit cavity The streamlines indicate the cores of the vortices A and C

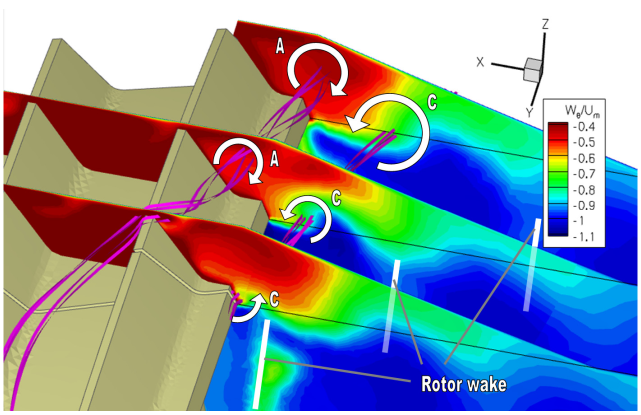

b) Relative tangential velocity in the shroud exit cavity

Figure 12 Flow in the shroud exit cavity (steady CFD)

mixing of the two flows with differing radial velocities creates high losses. In addition, the axial and tangential momenta of both flows are also quite different. Due to the turning in the rotor passage, the rotor exit flow has a high relative tangential velocity. Since there has been only a little turning (by viscous drag on the shroud and casing) of the shroud leakage flow, it has kept its low relative tangential velocity along the shroud leakage path. As a result, two streams of different tangential momentum have to mix in the shroud exit cavity. Figure 12a and b show the effect of this mixing with the help of the radial and the relative tangential velocity at three θ=const planes in the shroud exit cavity. In addition, streamlines that mark the cores of the shroud cavity vortex and the shroud trailing edge vortex are shown. On the downstream side of the shroud trailing edge vortex, main passage fluid enters the cavity with high tangential momentum and mixes with the shroud leakage flow. On the upstream side of the shroud trailing edge vortex, shroud leakage flow of low relative tangential momentum re-enters the main passage. This strong interaction between main passage flow and shroud leakage flow is also associated with high losses.

Model of the Over-Shroud Leakage Flow

The results from the flow visualisation, the PIV experiments and the numerical computations have revealed many details of the flow field within the cavities of the rotor shroud. The inter shroud gaps were found to be of decisive significance for the over shroud leakage flow. The observed flow field is much more complicated compared to that of a continuous shroud, where large circumferentially uniform vortices fill the shroud cavities.

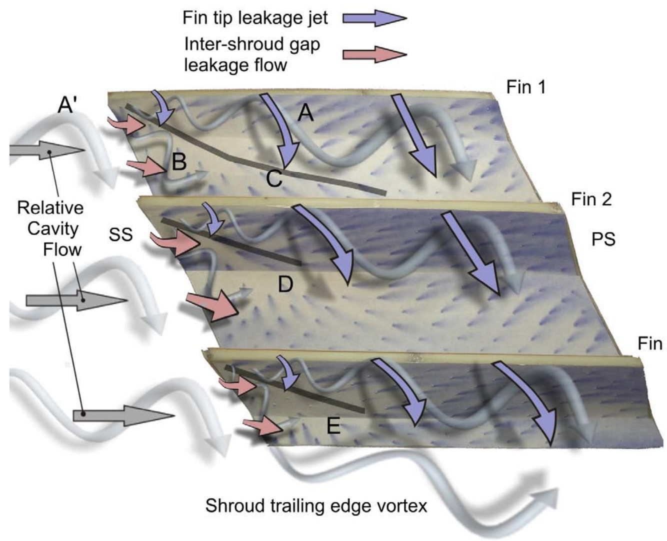

Figure 13 Experimental shroud surface flow visualisation and Model of flow structures in the shroud cavities

A simplified model of the shroud cavity flow is depicted in Figure 13. Near the pressure side of the shroud, the fin tip leakage jets drive large vortices filling the entire shroud cavities. These shroud cavity vortices pass the inter shroud gap over towards the adjacent shroud. In this process they interact with the leakage flow from the inter shroud gap and dissipate. The inter shroud gap leakage flow leads to a separation of the fin tip leakage jets from the casing. New shroud cavity vortices develop near the suction side of the shroud. Furthermore, small but intense vortices form near the inter shroud gap. The observed flow structures are shroud (blade) periodic. It was shown that they have negative effects on the discharge behaviour of the fin tip leakage flow. It is shown in the companion paper Lehmann et al. [1] that the presence of these vortices has also negative consequences for the thermal aspects of the over shroud leakage flow.

SUMMARY AND CONCLUSIONS

Endoscopic PIV measurements were carried out over the rotor shroud region in a low speed turbine rig incorporating a typical aero-engine HPT shrouded rotor blade. The results are presented along with numerical predictions obtained from steady and unsteady simulations conducted on identical stage geometry. The following are the notable findings and conclusions from the study reported in this paper.

The shroud inlet cavity shows the existence of a large single cavity vortex. Radial migration of fluid into the shroud inlet cavity is influenced by the stator and rotor blade pressure fields, with the latter playing a leading role. Furthermore, the circumferential inter-shroud gap was found to influence the inflow pattern relative to the rotor blade.

The flow in the first shroud cavity is characterised by three vortices namely the shroud cavity vortex, the shroud gap vortex and a third vortex generated from the shear layer formed at the backward facing step. The development of the former two is related to the interaction between the fin tip leakage jet and the leakage jet from the inter shroud gap. The separation of the fin tip leakage jet from the casing leads to an impingement of this flow on to the back face of Fin 1. The appearance of the shear layer vortex at the top modifies the discharge coefficient over Fin 2 thus causing a circumferential modulation in the leakage mass flow relative to the rotor.

The second cavity is dominated by a similar vortex system as in the first cavity. However, the larger size of this cavity (higher fins) encourages the dissipation of the above vortex thus reducing its impact on the cavity walls.

Three main vortical structures are identified in the shroud exit cavity namely the shroud cavity vortex formed by the fin tip leakage jet, the shroud gap vortex and the shroud trailing edge vortex. Whilst the effect of the first two vortices is to cause impingement on to the rear face of Fin 3, the shroud trailing edge vortex is mainly responsible for the circumferential and radial mixing of the main flow and the cavity flow with characteristically different radial and circumferential velocity components.

Finally, a schematic model of the shroud leakage flow mechanism describing the key flow features is suggested.

ACKNOWLEDGEMENTS

This research was conducted within the European research project AITEB-2, 6FP, AST4-CT-2005-516113. The authors wish to thank all members of the AITEB-2 consortium and the European Commission for funding this research work. In addition the authors are grateful for the cooperation with Vassilis Stefanis of ALSTOM regarding the generation of the computational mesh.

REFERENCES

[1] Lehmann, K., Kanjirakkad, V., R., Hodson, H. P., 2011 “Aerodynamic and Aerothermal investigation of the flow around an HPT Rotor Shroud: Heat Transfer and Cooling Effectiveness”, ASME Turbo Expo, GT2011-45979

[2] Pfau, A., Kalfas, A. I., Abhari, R. S., 2007, “Making Use of Labyrinth Interaction Flow”, ASME J. Turbomach. Vol. 129 164

[3] Porreca, L., Kalfas, A. I., Abhari, R. S., 2008, “Optimized Shroud Design for Axial Turbine Aerodynamic Performance”, J. Turbomach. 130

[4] Rosic, B., Denton, J. D., Curtis, E. M., 2008, “The Influence of Shroud and Cavity Geometry on Turbine Performance: An Experimental and Computational Study—Part I and Part II”, ASME J. Turbomach. 130

[5] Gier, J., Stubert, B., Brouillet, B., de Vito, L., 2005, “Interaction of Shroud Leakage Flow and Main Flow in a Three-Stage LP Turbine”, ASME Journal of Turbomach. Vol. 127, pp. 649-658.

[6] Giboni, A., Wolter, K., Menter, J. R., Pfost, H., 2004, “Experimental and Numerical Investigation into the Unsteady Interaction of Labyrinth Seal Leakage Flow and Main Flow in a 1.5-Stage Axial Turbine”, ASME IGTI Turbo Expo, GT2004-53024

[7] Kanjirakkad, V. P., Thomas, R. L., Hodson, H. P., Janke, E., Haselbach, F., Whitney, C., 2008 “Passive Shroud Cooling Concepts for HP Turbines: Experimental Investigations”, Journal of Turbomachinery, Vol. 130,1

[8] Janke, E., Haselbach, F., Whitney, C., Kanjirakkad, V., P., Thomas, R. L., Hodson, H. P., 2006 “Passive Shroud Cooling Concepts for HP Turbines: CFD based Design Approach”, ASME IGTI Turbo Expo, GT2006-91194

[9] Waschka, W., Wittig, S., Kim, S., Scherer, T., 1993 “Heat Transfer and Leakage in High-Speed Rotating Stepped Labyrinth Seals,” AGARD Conference Proceedings 527, Heat Transfer and Cooling in Gas Turbines

[10] Wittig, S., Jacobsen, K., Schelling, U., Kim, S., 1988, “Heat Transfer in Stepped Labyrinth Seals”, Journal of Engineering for Gas Turbines and Power, Vol. 110, pp. 63-69

[11] Haller, B. R., Hilditch, M. A., “External Heat Transfer on a Shrouded HP Gas Turbine Stage”, ASME IGTI Turbo Expo, GT2007-27168

[12] Lehmann, K., Thomas, R., Hodson, H. P., Stefanis, V., 2009, „Heat Transfer and Aerodynamics of Over-Shroud Leakage Flows in a High Pressure Turbine“, ASME Turbo Expo, GT2009-59531

[13] Rushton, G., J., 2003, "The Aerodynamics of Shrouded Multistage Turbines", PhD Thesis, University of Cambridge

